

Article

Quadrupedal Robots' Gaits Identification via Contact Forces Optimization

Gianluca Pepe ^{1,*}, Maicol Laurenza ¹, Nicola Pio Belfiore ² and Antonio Carcaterra ¹

¹ Department of Mechanical and Aerospace Engineering, Sapienza University of Rome, 00184 Rome, Italy; maicol.laurenza@uniroma1.it (M.L.); antonio.carcattera@uniroma1.it (A.C.)

² Department of Engineering, University of Roma Tre, via Della Vasca Navale 79, 00146 Rome, Italy; nicolapio.belfiore@uniroma3.it

* Correspondence: gianluca.pepe@uniroma1.it

Abstract: The purpose of the present paper is the identification of optimal trajectories of quadrupedal robots through genetic algorithms. The method is based on the identification of the optimal time history of forces and torques exchanged between the ground and the body, without any constraints on leg kinematics. The solutions show how it is possible to obtain similar trajectories to those of a horse's walk but obtaining better performance in terms of energy cost. Finally, a map of the optimal gaits found according to the different speeds is presented, identifying the transition threshold between the walk and the trot as a function of the total energy spent.

Keywords: gait optimization; quadrupedal robot; genetic algorithm; quadrupedal locomotion; evolutionary programming; optimal contact forces; cost of transport



Citation: Pepe, G.; Laurenza, M.; Belfiore, N.P.; Carcaterra, A. Quadrupedal Robots' Gaits Identification via Contact Forces Optimization. *Appl. Sci.* **2021**, *11*, 2102. <https://doi.org/10.3390/app11052102>

Academic Editor:

Alessandro Gasparetto

Received: 31 December 2020

Accepted: 21 February 2021

Published: 27 February 2021

Publisher's Note: MDPI stays neutral with regard to jurisdictional claims in published maps and institutional affiliations.



Copyright: © 2021 by the authors. Licensee MDPI, Basel, Switzerland. This article is an open access article distributed under the terms and conditions of the Creative Commons Attribution (CC BY) license (<https://creativecommons.org/licenses/by/4.0/>).

1. Introduction

Nature has always been a source of inspiration for engineers and scientists who tried to replicate or mimick natural bio-mechanisms. In fact, this can be a smart strategy, since any natural living being is a highly optimized system over millions of years of evolution [1–3]. Magnificent examples of engineering bio-inspired devices date from very ancient Magna Greece times, as the Archita's dove automaton, and a large number of automata within the Erone's tradition. The masterful Leonardo's machines, such as the lion or the knight automaton, or the flying machines, some inspired by the flapping wings of birds, are also astonishing examples.

To date, the development of automatic systems, in particular quadrupedal robots, has found great motivation in the field of human assistance. To assist and cooperate with humans, robots must be able to move easily in workplaces originally designed according to human needs [4]. For example, climbing stairs, avoiding obstacles, or opening doors [5,6]. Among the many technical difficulties to be faced and solved, one of the most important aspects is related to portability and its duration. This scenario justifies the need to optimize the power and energy of locomotion to make these systems more efficient, compact, characterized by limited energy consumption, and using small size and weight actuators.

Interesting questions arise: is it possible to conceive more efficient quadrupeds than those proposed by nature? Is it possible to disclose a different kind of gaits for a quadrupedal mechanism as the product of a strict optimization process? For example, depending on speed, energy consumption, or jerk minimization. Many engineers and robot designers assume the gait of animals is optimal since they would have been able to survive the competition and natural selection [7–10]. For this reason, the quadrupedal robot tends to be designed inspired by the examples of nature [11,12]. However, biological kinematics of locomotion is not reproducible directly by a legged robot, since biological muscles are extraordinarily efficient components, and animals can produce energy for their actuation by grabbing nutritive elements from the environment, transformed into actuation

energy by a digestive process. This permits them to have a relatively light energy storage system. Moreover, artificial sensors are still inferior, in terms of number, miniaturization, and sensitivity against the ones owned by animals [13].

To date, designers tend to create robots that resemble nature as closely as possible, such as imposing specific gaits such as walking, trotting, or galloping and developing mathematical optimization processes that only concern sub-systems, to overcome the technological limitations [14,15]. There are many different approaches for performing the optimization. In [16], for example, the authors use harmonic functions to describe foot trajectory and tune some parameters such as amplitude, phase, and frequency. In [17,18] the authors generate leg trajectories for overcoming small terrain irregularities by optimizing consumed energy. In [19] the authors optimize contact forces to walk on a high-slope terrain, but the gait is imposed a priori.

Evolutionary computation, such as genetic algorithms (GAs), is often a natural choice for the gait optimization of legged robots since it uses optimization methods based on evolutionary theory [20]. Also, the controls of the mentioned cases, tend to mimic or approach the natural movement of the quadrupeds found in nature. Typical controls are central pattern generators [21,22], hybrid zero dynamics [23], or the usual PD [24].

The present work breaks from all the problems relating to technological limitations and lays the foundations of how it is possible to identify, a priori, optimal gaits through parametric optimization algorithms. The authors propose an algorithm that does not depend either on the kinematic chains of the legs or power actuators. The method directly handles the contact forces that the hypothetical legs exchange with the ground, identifying the sequence that guarantees minimum energy consumption and smooth motion during a single stride cycle. The genetic algorithm (GA) is used to minimize the kinetic and potential energy as well as restraining the jerk, identifying the optimal profile of normal and friction forces. The equations of motion are solved through some periodicity constraints of the gait, thus ensuring a stable and continuous motion. The optimal gaits identified are very similar to those found in nature. The authors have optimized the gait of a heavy and bulky horse-like robot, obtaining a walking trot as the optimal gait, and then comparing it with experimental data from real horses. Additionally, a gait transition analysis is performed as a function of locomotion speed and gait cycle length, showing why it is convenient to walk or trot.

The paper is organized as follows: Section 2 describes the dynamic model and ground reaction force shapes; Section 3 defines the optimization parameters and objective functions while introducing stability constraints to assure a periodic motion; Section 4 provides the resulting optimal gait, along with the comparison with horse experiments and identification of gait transition; Section 5 discusses the limitations and future challenges of the method and finally the conclusions.

2. Mathematical Model for the Gait Optimization

The considered quadrupedal model is sketched in Figure 1, where the body, suspended on four legs, transmits forces and moments thanks to the interaction with the ground.

The optimization model proposed in this paper consists of an optimal gait identification, capable of moving the quadrupedal body through the succession of four alternating thrusts generated by legs with some desirable characteristics. This approach is innovative. In fact, the kinematic linkages and actuators of the leg mechanism are not directly involved but left to a second engineering phase of design, not investigated in the present paper.

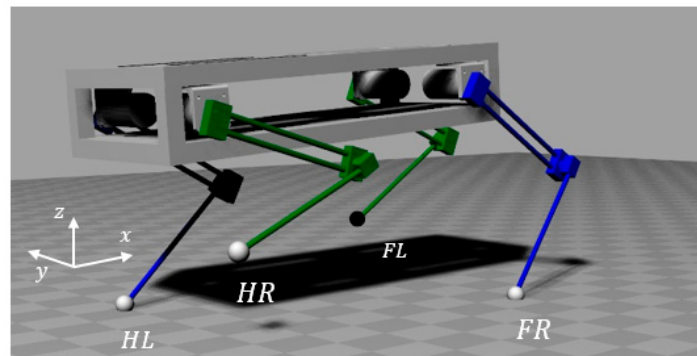


Figure 1. 3D view of the quadruped.

The legs are labelled as *FL* (front left), *FR* (front right), *HL* (hind left), *HR* (hind right). The period during which a single leg maintains its contact with the ground is the *contact phase* (*CP*), while the one during which the leg is flying in the air moving towards the next contact point, is the *swing phase* (*SP*). In general, these times can be set differently for each leg.

The legs sequencing, sketched in Figure 2, originates a periodic motion of each leg, of period T . The time at which each leg touches the ground is $t_i \in [0, T]$, where $i = FR, FL, HR, HL$. The time duration of the contact phase is T_i , and the time duration of the swing phase is $T - T_i$.

Newton–Euler equations of rigid body dynamics are:

$$\begin{aligned} m \ddot{\mathbf{r}} &= \mathbf{f}_e \\ \mathbf{I} \dot{\boldsymbol{\omega}} &= \mathbf{m}_e - \boldsymbol{\omega} \times (\mathbf{I} \boldsymbol{\omega}) \\ \dot{\boldsymbol{\theta}} &= \mathbf{E}(\boldsymbol{\theta}) \boldsymbol{\omega} \end{aligned} \tag{1}$$

where the first equation holds in the fixed reference frame, the second in the body reference frame (principal inertia axes), $\mathbf{r} = [x, y, z]$ identifies the gravity center position of the quadruped body of total mass m , \mathbf{f}_e is the total external force, $\mathbf{I} = \text{diag}[I_x, I_y, I_z]$ the matrix of inertia, \mathbf{m}_e is the total external moment, $\boldsymbol{\theta} = [\psi, \theta, \phi]$, the Tait–Bryan angles (yaw pitch and roll), $\boldsymbol{\omega}$ is the angular velocity, and \mathbf{E} is the Jacobian matrix.

Assuming small pitch and roll angles and vanishing yaw, the equations can be reduced into the same fixed reference frame:

$$\begin{aligned} m \ddot{x} &= F_x \\ m \ddot{y} &= F_y \\ m \ddot{z} &= F_z \\ I_x \ddot{\phi} &= M_x \\ I_y \ddot{\theta} &= M_y \end{aligned} \tag{2}$$

where F_x, F_y, F_z, M_x, M_y are the total force and moment transmitted by the four legs *FR*, *FL*, *HR*, and *HL*, respectively.

When the quadruped moves on the ground, the leg–ground contact produces a reaction force. Its vertical component F_z supports the quadrupedal weight, the horizontal component F_x drives the longitudinal motion of the body, and F_y affects the lateral body oscillations.

The vertical force F_{z_i} for each leg acts only in the *CP*; that implies $F_{z_i}(t_i) = 0$ and $F_{z_i}(t_i + T_i) = 0$, that is, its time history, during the *CP*, starts and ends with vanishing values, associated with the incipient contact and incipient detachment of the leg with and from the ground, respectively. The force–time history along the *CP* is identified through three additional points $[P_{1,i}; P_{2,i}; P_{3,i}]$ (besides the two previously identified) and is fitted by a suitable spline (Figure 3a).

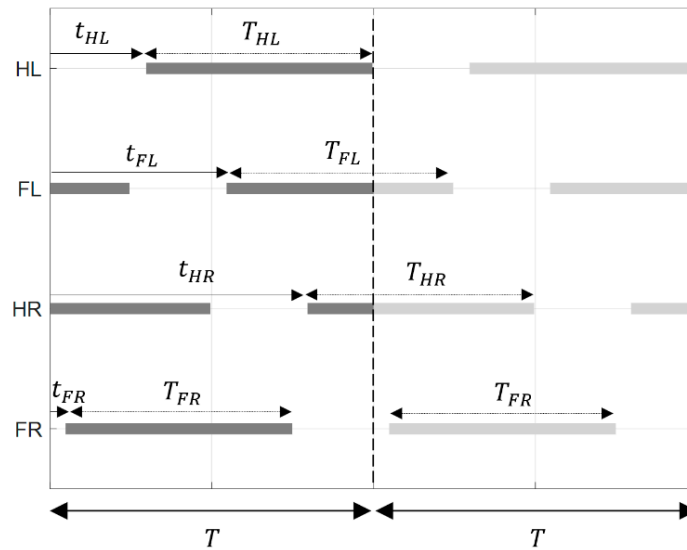


Figure 2. Time diagram of the quadruped’s locomotion over the entire period T shows the times t_i at which each leg touches the ground and the time duration T_i of each contact phase. The subscripts $i = FR, FL, HR, HL$ are FL (front left), FR (front right), HL (hind left), and HR (hind right).

The longitudinal and lateral ground reactions for each leg are assumed to belong to the static friction cone. With this assumption, any contact slip condition is absent, and the contact model is purely conservative. Therefore:

$$\sqrt{F_{x_i}^2 + F_{y_i}^2} \leq \mu_s F_{z_i} \tag{3}$$

where μ_s is the static friction coefficient.

For the planar forces F_{x_i} and F_{y_i} , one can introduce suitable constitutive relationships (Figure 3). Several experiments available in the technical literature [25,26] suggest the following gait dynamics for leg locomotion. When the leg touches the ground, in the first phase, a backward longitudinal reaction brakes the body run, followed by a second phase, in which the leg accelerates the body through a forward longitudinal reaction force (Figure 3d). Moreover, the amplitude of the longitudinal reaction force is roughly proportional to the normal vertical force. A similar force trend holds for the lateral force that is responsible for the unavoidable lateral staggering of the quadruped’s body. For both longitudinal and lateral forces, one can introduce the suitable factorization form as constitutive relationships:

$$\begin{aligned} F_{x_i}(t) &= \mu_{x_i}(t)F_{z_i}(t) \\ F_{y_i}(t) &= \mu_{y_i}(t)F_{z_i}(t) \end{aligned} \tag{4}$$

that use the proportionality of the planar forces to the vertical one. Moreover, the role of the factors $\mu_{x_i}(t)$, $\mu_{y_i}(t)$ is that of reproducing the time history of the planar force, $F_{x_i}(t)$ or $F_{y_i}(t)$, as reported in Figure 3c,d, modulating the amplitude of the vertical reaction $F_{z_i}(t)$. In particular, $\mu_{x_i}(t)$, $\mu_{y_i}(t)$ are vanishing outside of the CP. Within the CP, in the first part of the contact, $\mu_{x_i}(t)$ takes negative values to reproduce the braking effect, while, in the second part, it becomes positive, to reproduce the acceleration effect.

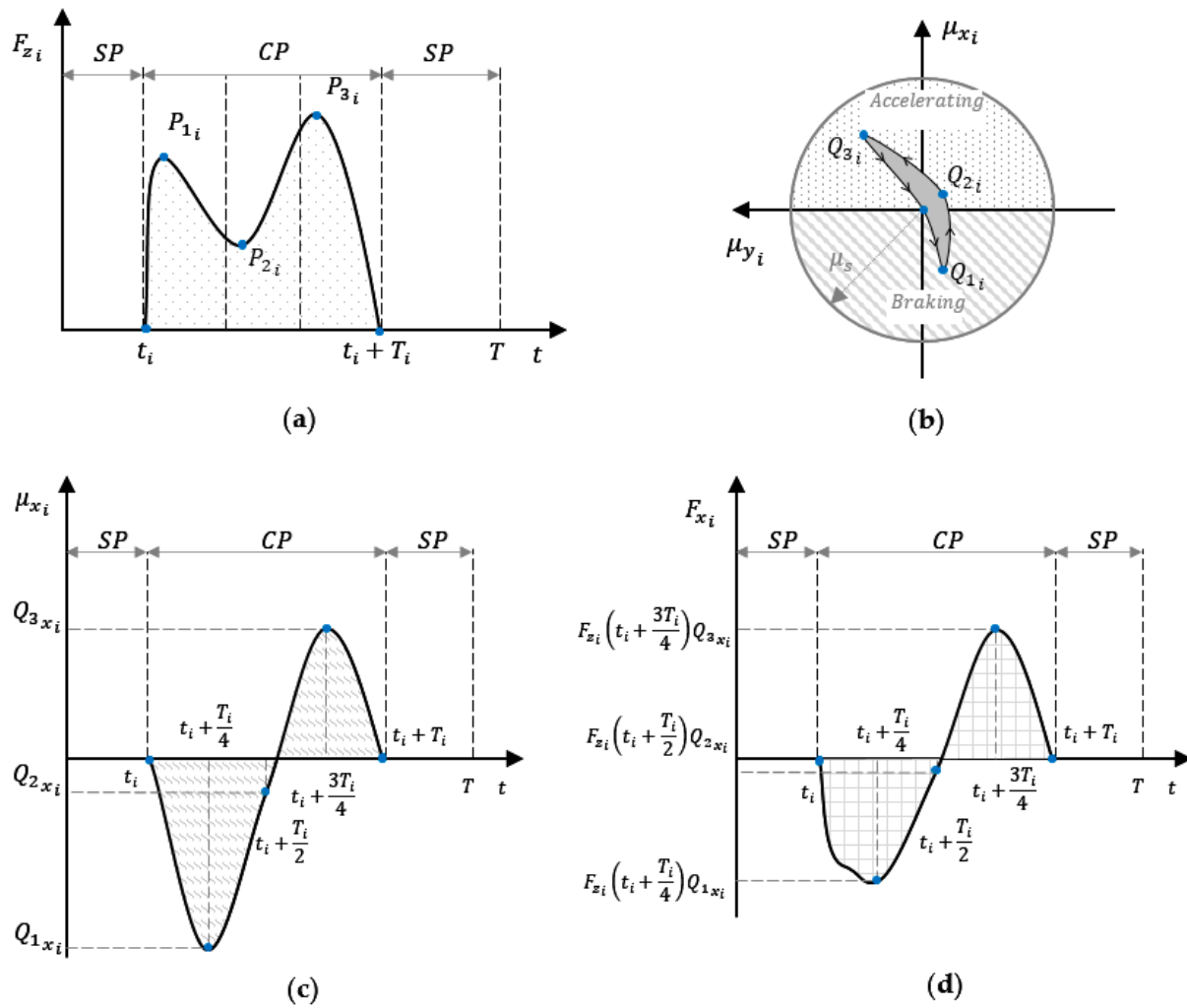


Figure 3. (a) Vertical ground force; (b) trend of the coefficient of adhesion inside the static friction cone; (c) longitudinal adhesion coefficient as a function of time; and (d) longitudinal ground force.

Combining Equations (4) and (3), the two modulating factors must satisfy the condition:

$$\sqrt{\mu_{x_i}^2 + \mu_{y_i}^2} \leq \mu_s \tag{5}$$

Looking at Figure 3b, this implies that at any time the point $Q_{j_i} [\mu_{x_{j_i}}(t), \mu_{y_{j_i}}(t)]$ remains confined in the circle of radius μ_s over the plane $\mu_{x_i}(t), \mu_{y_i}(t)$. Moreover, we assume a correlation between the modulating factors during the gait. This implies, concerning Figure 3b, the point $Q_{j_i} [\mu_{x_{j_i}}(t), \mu_{y_{j_i}}(t)]$ describes a closed curve in the plane $\mu_{x_i}(t), \mu_{y_i}(t)$ as time is spent, and Q completes the loop in a period T . More precisely, the time histories of $\mu_{x_i}(t), \mu_{y_i}(t)$ are determined by a spline passing through the points $[Q_{1_i}; Q_{2_i}; Q_{3_i}]$ selected by the designer within the contact cone (see Figure 3b).

The expressions for the moments M_x and M_y follow directly from the leg’s reactions. From Figure 4, let’s consider, for example, the FR foot at the incipient contact phase and foot position (x_{FR}, y_{FR}, z_{FR}) :

$$\begin{aligned} M_y &= F_x \Delta z_{FR} - F_z \Delta x_{FR} \\ M_x &= F_y \Delta z_{FR} + F_z \Delta y_{FR} \end{aligned} \tag{6}$$

where $\Delta x_{FR}(t) = x_{FR} - x$, $\Delta z_{FR}(t) = z_{FR} - z$ and $\Delta y_{FR} = y_{FR} - y$.

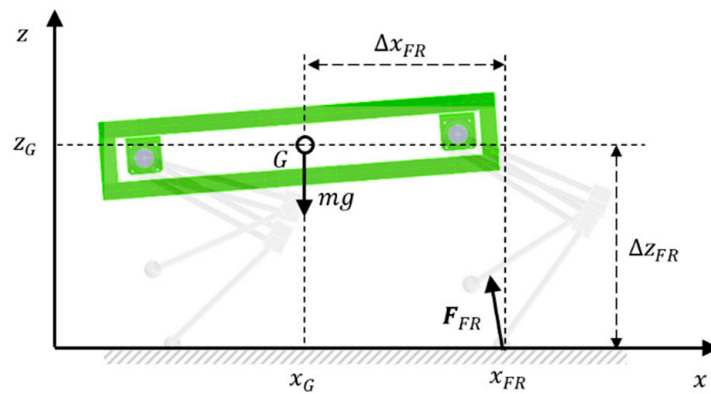


Figure 4. Point of application of the leg force FR and distances Δx_{FR} and Δz_{FR} referred to the center of gravity G.

3. Optimization Model

Usually, in the legged locomotion, the stability of a gait is guaranteed by using a criterion such as zero-moment point [27,28]. Other studies face the stability problem with the Poincare map [29,30] or ground reference points [31]. In this paper, unlike the classical approaches, the gait stability is guaranteed by satisfying periodic limit cycle conditions.

The optimization operates over a single period T using a genetic algorithm (GA) which provides the stride length, frequency, and velocity, and additionally the time history of the contact forces. Therefore, a vector of gait parameters p_{GA} is optimized by using the GA algorithm. Let us explicitly set p_{GA} . The relative phases of the leg motion are t_i , the normalized time duration T_i of the CP is $\beta_i = \frac{T_i}{T}$, the time history of the normal, longitudinal and lateral contact forces are determined by the interpolation of the points P_j and Q_j with $j = 1, 2, 3$, respectively. Therefore:

$$p_{GA} = [t_i, \beta_i, P_{j_i}, Q_{j_i}] \tag{7}$$

The structure of the optimization process involves the optimal vector p_{GA} and, using several constraints derived from the equations of motion, it looks for solutions that minimize a multi-objective cost function related to the dissipated energy and looking for smooth forces trends. Let us examine in detail these constraints.

Note, as a preliminary consideration, that we can impose the continuity kinematic conditions over the stride period:

$$\begin{aligned} y(0) &= y(T); & z(0) &= z(T) \\ \dot{x}(0) &= \dot{x}(T); & \dot{y}(0) &= \dot{y}(T); & \dot{z}(0) &= \dot{z}(T) \\ \phi(0) &= \phi(T); & \theta(0) &= \theta(T) \\ \dot{\phi}(0) &= \dot{\phi}(T); & \dot{\theta}(0) &= \dot{\theta}(T) \end{aligned} \tag{8}$$

Moreover, the average speeds over the period T are $\bar{\dot{x}} = V, \bar{\dot{y}} = 0, \bar{\dot{z}} = 0, \bar{\dot{\theta}} = 0, \bar{\dot{\phi}} = 0$, where V is the average longitudinal speed of the quadruped body.

We start with the vertical equation of motion (an identical procedure applies to the other equations of motion) that produces:

$$m\ddot{z} = \sum_i F_{z_i}(P_{j_i}) - mg \quad \rightarrow \quad \dot{z} = \frac{1}{m} \int_0^t \sum_i F_{z_i}(P_{j_i}) dt - gt + C \tag{9}$$

where g is the gravity acceleration and C is an integration constant. Therefore:

$$\dot{z}(T) = \frac{1}{m} \int_0^T \sum_i F_{z_i}(P_{j_i}) dt - gT + C \tag{10}$$

and

$$\dot{z}(0) = C \tag{11}$$

Using the condition $\dot{z}(0) = \dot{z}(T)$, it follows:

$$\frac{1}{T} \int_0^T \sum_i F_{z_i}(P_{j_i}) dt = mg \tag{12}$$

The force-time history is set by randomly selecting the point P_{j_i} by the GA and using a spline interpolation. Further integration of Equation (10) produces:

$$\begin{aligned} \dot{z}(t) &= \frac{1}{m} \int_0^t \sum_i F_{z_i}(P_{j_i}) d\tau - gt + \dot{z}(0) \rightarrow z(t) \\ &= \frac{1}{m} \int_0^t \int_0^\tau (\sum_i F_{z_i}(P_{j_i}) - mg) dt d\tau + \dot{z}(0)t + z(0) \end{aligned} \tag{13}$$

and:

$$z(T) = \frac{1}{m} \int_0^T \int_0^\tau (\sum_i F_{z_i}(P_{j_i}) - mg) dt d\tau + \dot{z}(0)T + z(0) \tag{14}$$

Using the periodicity condition $z(0) = z(T)$, it follows:

$$\dot{z}(0) = -\frac{1}{mT} \int_0^T \int_0^\tau (\sum_i F_{z_i}(P_{j_i}) - mg) dt d\tau \tag{15}$$

Equation (15) automatically satisfies the condition of zero average speed $\bar{\dot{z}} = 0$. In fact:

$$\begin{aligned} \dot{z}(t) &= \frac{1}{m} \int_0^t \sum_i F_{z_i}(P_{j_i}) d\tau - gt + \dot{z}(0) \rightarrow \bar{\dot{z}} \\ &= \frac{1}{mT} \int_0^T \int_0^\tau (\sum_i F_{z_i}(P_{j_i}) - mg) dt d\tau + \dot{z}(0) = 0 \end{aligned} \tag{16}$$

The longitudinal dynamics takes into account two inertia effects: one related to the longitudinal motion of the robot body mass m_B , and the second due to the reciprocating motion of the legs of mass m_{p_i} . The total robot mass m is consequently:

$$m = m_B + \sum_i m_{p_i} \tag{17}$$

Let us make the point about the leg motion. Looking at Figure 5, it appears that, during the contact phase, the horizontal speed of the leg is negative, and becomes positive during the swing phase. Therefore, along the gait period, the leg mass behaves as an oscillator that, attached to the primary body mass, generates a back and forth horizontal inertia force.

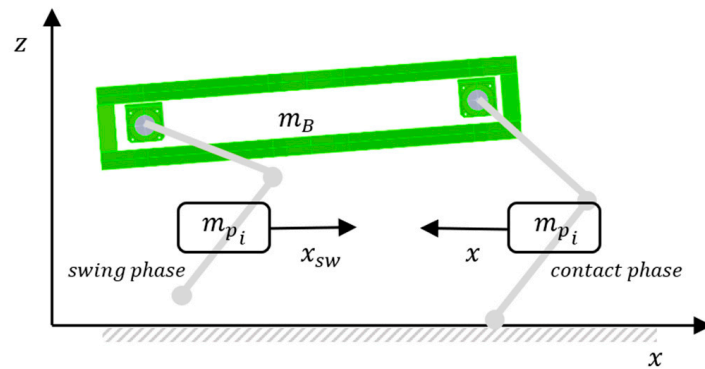


Figure 5. Illustration of the reciprocating longitudinal leg motion during the swing and contact phases, respectively.

The mathematical counterpart of this physical behaviour appears as follows:

$$m_B \ddot{x} - \sum_i m_{p_i} w_i(t) \ddot{x} = \sum_i F_{x_i} - \sum_i m_{p_i} (1 - w_i(t)) \ddot{x}_{sw_i} \tag{18}$$

x_{sw_i} describes the leg mass longitudinal motion during the swing phase. The term $m_{p_i} (1 - w_i(t)) \ddot{x}_{sw_i}$ takes into account the inertia force during the swing phase, while, complementarily, $m_{p_i} w_i(t) \ddot{x}$ accounts for the added mass effect during the contact phase, within which the leg motion depends essentially on the body motion. The switch function $w_i(t)$ is defined as:

$$w_i(t) = \begin{cases} 1 & \text{if the } i^{\text{th}} \text{ leg is in CP} \\ 0 & \text{if the } i^{\text{th}} \text{ leg is in SP} \end{cases} \tag{19}$$

that activates alternatively the inertia effects of the contact and swing phase, respectively. The swing motion $x_{sw_i}(t)$ is designed through β_i and T by using a spline with initial and final slope equal to the average body velocity V (as an example see Figure 6).

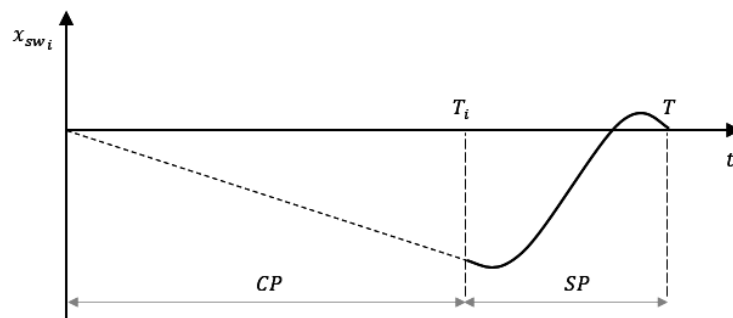


Figure 6. An example of the time history of x_{sw_i} of the leg.

The analogous Equation (12) is determined for the longitudinal motion using the condition $\dot{x}(0) = \dot{x}(T)$:

$$\int_0^T \frac{\sum_i F_{x_i}(P_{j_i}, Q_{x_{j_i}}) - \sum_i m_{p_i} (1 - w_i(t)) \ddot{x}_{sw_i}}{m_B - \sum_i m_{p_i} w_i(t)} dt = 0 \tag{20}$$

Then the average speed $\bar{\dot{x}} = V$ over the period T is:

$$\bar{\dot{x}} = V = \frac{1}{T} \int_0^T \int_0^\tau \frac{\sum_i F_{x_i}(P_{j_i}, Q_{x_{j_i}}) - \sum_i m_{p_i} (1 - w_i(t)) \ddot{x}_{sw_i}}{m_B - \sum_i m_{p_i} w_i(t)} d\tau dt + \dot{x}(0) \tag{21}$$

that, together with the periodicity condition, produces:

$$\dot{x}(0) = \dot{x}(T) = V - \frac{1}{T} \int_0^T \int_0^\tau \frac{\sum_i F_{x_i}(P_{j_i}, Q_{x_{j_i}}) - \sum_i m_{p_i}(1 - w_i(t))\ddot{x}_{sw_i}}{m_B - \sum_i m_{p_i}w_i(t)} d\tau dt \quad (22)$$

If the same procedure is applied to the lateral motion, it follows:

$$m\ddot{y} = \sum_i F_{y_i}(P_{j_i}, Q_{y_{j_i}}) \rightarrow \int_0^T \sum_i F_{y_i}(P_{j_i}, Q_{y_{j_i}}) dt = 0 \quad (23)$$

derived under the condition $\dot{y}(0) = \dot{y}(T)$. Using the other periodicity condition $y(0) = y(T)$, and $\dot{\bar{y}} = 0$, we obtain:

$$\dot{y}(0) = -\frac{1}{mT} \int_0^T \int_0^\tau \sum_i F_{y_i}(P_{j_i}, Q_{y_{j_i}}) dt d\tau \quad (24)$$

We can apply the same procedure to the remaining cardinal equations. Using the conditions $\dot{\theta}(0) = \dot{\theta}(T)$, $\dot{\phi}(0) = \dot{\phi}(T)$, the following constraints are obtained:

$$\begin{aligned} \int_0^T \sum_i M_{y_i}(x_0) dt &= 0 \\ \int_0^T \sum_i M_{x_i}(y_0) dt &= 0 \end{aligned} \quad (25)$$

These can be solved in closed form in terms of the initial conditions x_0 e y_0 . The arms of the moments are:

$$\begin{aligned} \Delta x_i(t, x_0) &= x_i(t) - x(t, x_0) \\ \Delta y_i(t, y_0) &= y_i(t) - y(t, y_0) \\ \Delta z_i(t, z_0) &= z_i - z(t, z_0) \end{aligned} \quad (26)$$

Assuming a flat ground, $z_i = 0$, and

$$\begin{aligned} x(t, x_0) &= \int_0^t \int_0^\tau \frac{F_x}{m_B - \sum_i m_{p_i}w_i(t)} dt d\tau + \dot{x}_0 t + x_0 \\ y(t, y_0) &= \frac{1}{m} \int_0^t \int_0^\tau F_y dt d\tau + \dot{y}_0 t + y_0 \\ z(t, z_0 = h) &= \frac{1}{m} \int_0^t \int_0^\tau (F_z - mg) dt d\tau + \dot{z}_0 t + h \end{aligned} \quad (27)$$

Finally, using again the same technique with the conditions $\phi(0) = \phi(T)$, $\theta(0) = \theta(T)$, the final equations yield:

$$\begin{aligned} \dot{\theta}(0) = \dot{\theta}(T) &= -\frac{1}{I_y T} \int_0^T \int_0^\tau M_y(x_0) dt d\tau \\ \dot{\phi}(0) = \dot{\phi}(T) &= -\frac{1}{I_x T} \int_0^T \int_0^\tau M_x(y_0) dt d\tau \end{aligned} \quad (28)$$

The previous constraints are based on the linear approximation (see Equation (2)) of the equations of motion, and they provide the initial guess of the kinematic variables at the initial and final times, 0 and T. Moreover, the force and the moments, through their

spline approximations, satisfy the set of conditions from (7) to (27). With this starting guess, we can solve the following iterative nonlinear optimization problem:

$$\begin{aligned}
 & \text{minimize} && \boldsymbol{\omega}(0) - \boldsymbol{\omega}(T) = \mathbf{0}_{3 \times 1} \\
 & && \boldsymbol{\theta}(0) - \boldsymbol{\theta}(T) = \mathbf{0}_{3 \times 1} \\
 & \text{subject to} && \dot{\boldsymbol{\omega}} = \mathbf{m}_e - \boldsymbol{\omega} \times (\mathbf{I}\boldsymbol{\omega}) \\
 & && \dot{\boldsymbol{\theta}} = \mathbf{E}(\boldsymbol{\theta})\boldsymbol{\omega} \\
 & && |\boldsymbol{\omega}| < \boldsymbol{\omega}_{max} \\
 & && |\boldsymbol{\theta}| < \boldsymbol{\theta}_{max} \\
 & \text{initial guess} && \boldsymbol{\theta}_0 = [\theta_0, \phi_0, \psi_0]^T = [0, 0, 0]^T \\
 & && \boldsymbol{\omega}_0 = [\dot{\theta}_0, \dot{\phi}_0, 0]^T \\
 & && \mathbf{r}_0 = [x_0, y_0, z_0]^T
 \end{aligned} \tag{29}$$

The unknown vector to be determined is $\mathbf{p}_{NLP} = [\theta_0, \phi_0, \psi_0, \dot{\omega}_{x_0}, \dot{\omega}_{y_0}, \dot{\omega}_{z_0}, x_0, y_0, z_0]$. Figure 7 illustrates the flow chart of the GA solution's scheme. The setting of the GA which led to good balancing between learning and overfitting is a size population of 50 individuals, 110 generations, a crossover of 80% and mutation of 1%. Specifically, the genetic algorithm with multi-objective optimization is used for which simultaneous optimization of multiple, often competing, objectives take place [32,33]. The related pseudocode is shown below:

Algorithms 1 Pseudo code for the gait optimization algorithm.

```

1:  t ← 0
2:  Initialization parameters [T, V, m, Ix, Iy, Iz, L, h, mp]
3:  GA random population initialization of  $\mathbf{p}_{GA}$  vector
4:  While {GA's stop criterion is not met}
5:      Vertical ground force definition with continuity kinematic constraints (periodicity condition)
6:      Longitudinal and lateral forces with continuity kinematic and static friction cone constraints
7:      Torques with continuity kinematic constraints in the linear case (small angles)
8:      Initialization guess parameters for Nonlinear Programming
9:      Evaluate Objective function for Nonlinear Programming
10: While {Nonlinear Programming's stop criterion is not met and the constraints are satisfied}
11:     Sequential Quadratic Algorithm
12:     Evaluate Objective function
13: Endwhile
14:     Evaluate fitness function for each individuals
15:     Select of the individuals
16:     Recombine of the individuals
17:     Mutate of the individuals
18:     Generations of new population
19:     t ← t + 1
20: Endwhile

```

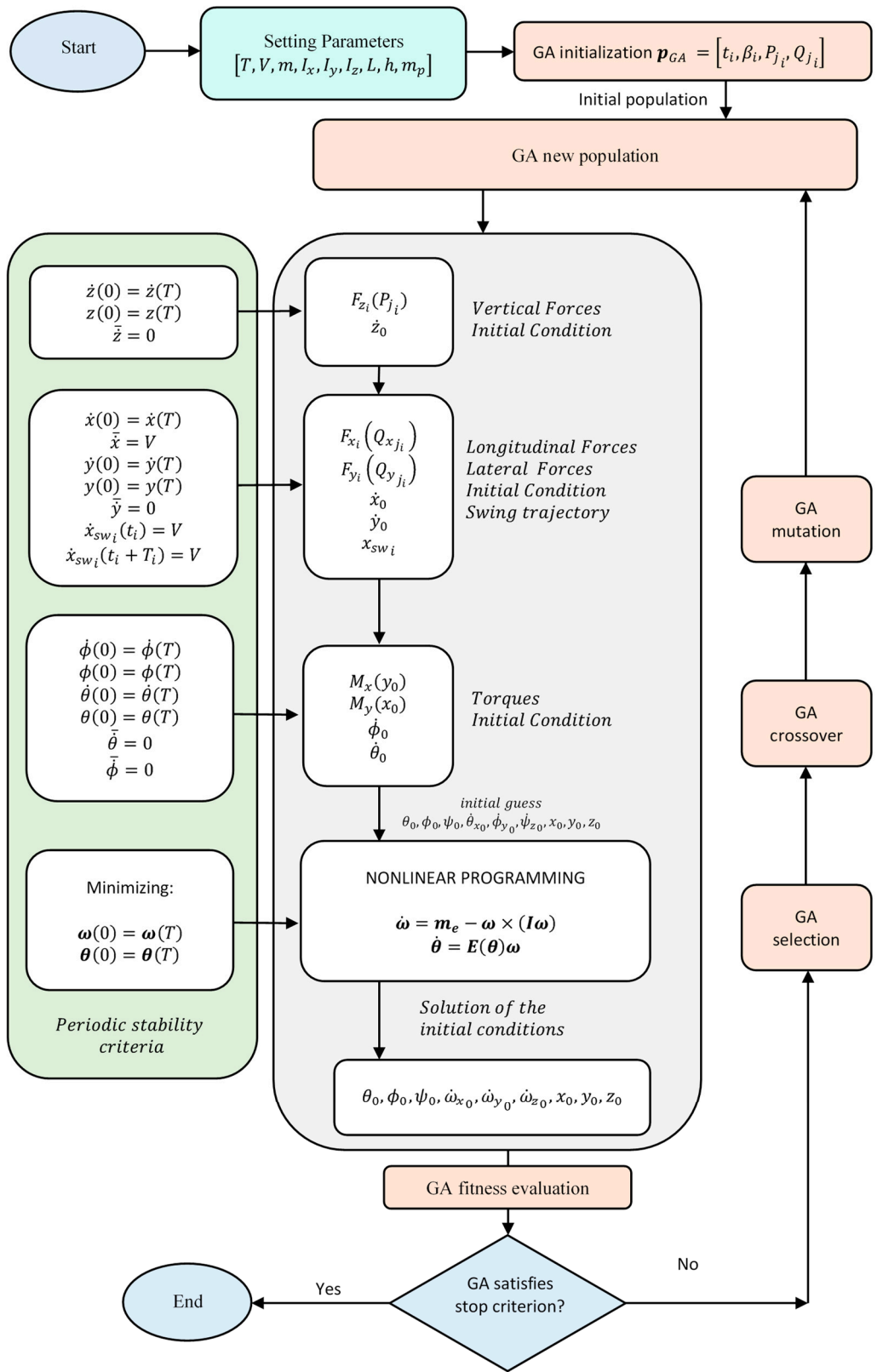


Figure 7. Optimization diagram of the genetic algorithm (GA) algorithm.

Eventually, we introduce the multi-objective function to be minimized for the most efficient gait. The GA's fitness function is defined through the total specific energy E_d , that is, the energy per traveled distance $x(T) - x_0$ over the period, and the ground reaction jerk J_{GRF} .

The specific energy E_d includes the mechanical energy of the body and the swinging leg energy:

$$E_d = \frac{1}{x(T) - x_0} \int_0^T |F_x \dot{x}| + |F_y \dot{y}| + |F_z \dot{z}| + |M_x \dot{\phi}| + |M_y \dot{\theta}| + |mg \dot{z}| + \left| \left(\sum_i m_{p_i} (1 - w_i(t)) \ddot{x}_{sw_i} \right) \dot{x}_{sw_i} \right| dt \tag{30}$$

One can expect power fluctuations along the period with positive and negative values, perfectly balanced since these fluctuations have zero average (the system is conservative). Since E_d integrates the absolute value of the power, it measures the intensity of the power fluctuations. Requiring a small value for E_d means asking for small fluctuations of the power, which implies a benefit in terms of the actuator dimensions and power and thus of energy consumption. On the other hand, the request of a small jerk J_{GRF} assures traditionally smooth contact forces:

$$J_{GRF} = \frac{1}{T} \int_0^T \| \dot{F} \| dt \tag{31}$$

where $F = [F_x; F_y; F_z]$.

Multi-objective optimization is used to determine the Pareto frontier, the set of solutions that provides the optimal trade-off between the two criteria.

4. Results

4.1. Optimal Gait Solution

For certain optimization variable sets p_{GA} , the solver may not converge, or the solution may be unrealistic or impractical. A maximum foot stride s_{max} has been imposed to avoid solutions that required unrealistic leg dimensions. The condition was applied to the upper bound of the duty factor: $\beta_{i_{max}} = \frac{s_{max}}{VT}$, where V is the mean target speed of the simulation:

$$0 < \beta_i \leq \beta_{i_{max}} \tag{32}$$

The optimization finds an efficient gait (in the sense specified in the previous section) that moves the body at an average speed of 1.35 m/s, with a gait period T of 1 s. The mass properties of the body are selected considering the characteristic parameters of quadrupeds in nature, in particular horses (Table 1, see reference [34]). In addition, some simplification but reasonable assumptions are made, namely: $\beta_{FR} = \beta_{FL} = \beta_F$, $\beta_{HR} = \beta_{HL} = \beta_H$, $F_{z_{FR}} = F_{z_{FL}}$, $F_{z_{HR}} = F_{z_{HL}}$, $F_{x_{FR}} = F_{x_{FL}}$, $F_{x_{HR}} = F_{x_{HL}}$, $F_{y_{FR}} = -F_{y_{FL}}$, and $F_{y_{HR}} = -F_{y_{HL}}$. The obtained solutions are plotted in Figure 8, where a correlation between the energy cost and contact-forces jerk is shown (Pareto frontier). The resulting gaits present a specific leg sequence classified as walk and trot gaits. In nature, walking gaits involve overlapping contact phase such that $\beta > 0.5$. In particular, in a trot gait, the diagonal forelimb and hindlimb move in phase, while in a walking gait the limbs have a lag of 0.25 between the two legs.

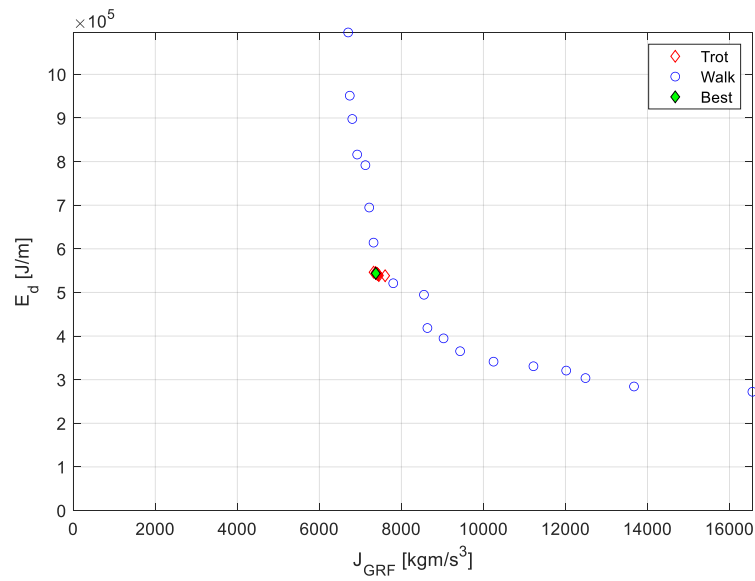


Figure 8. Pareto curve of optimal gaits for $V = 1.35$ m/s and $T = 1$ s.

The best solution according to the Pareto frontier is presented in Figure 9. It can be seen how the body keeps a steady longitudinal speed \dot{x} , about the target speed of $V = 1.35$ m/s, maintaining a stable and restrained attitude and assuring the periodicity constraints.

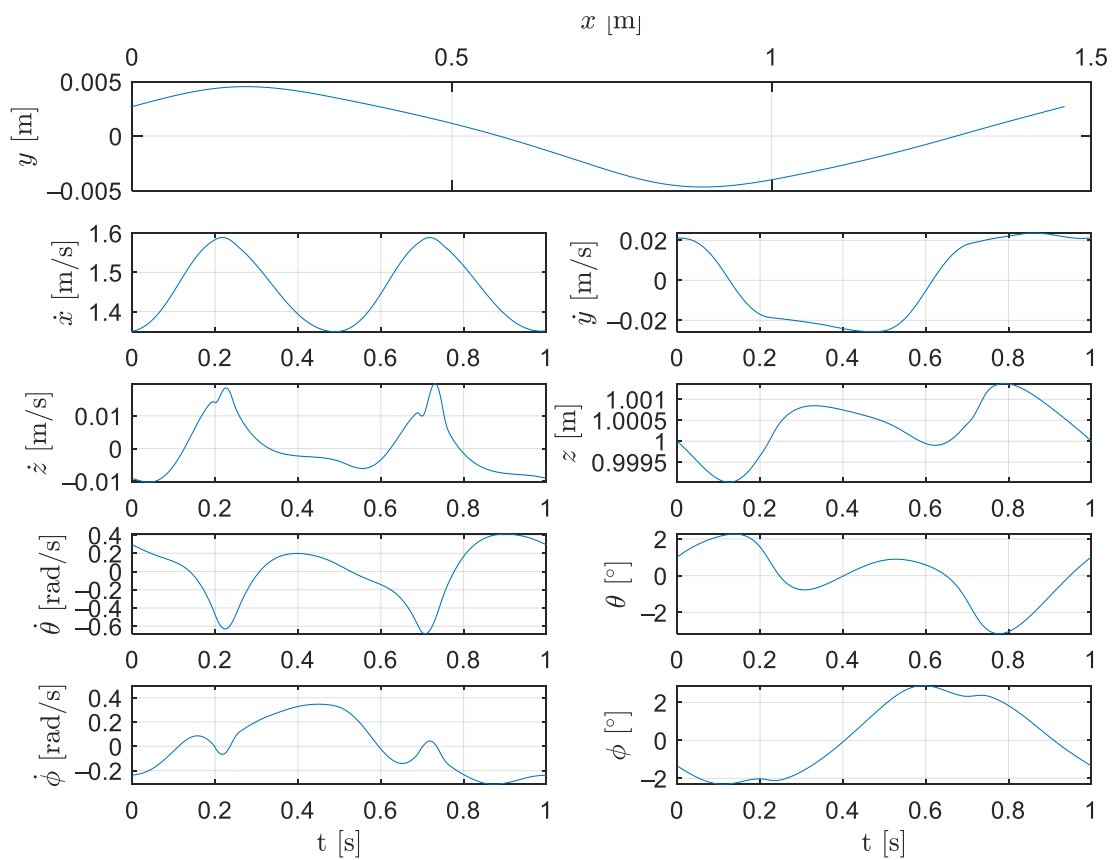


Figure 9. Trajectory and attitude of the selected optimal solution.

This case is classified as a walking trot since it presents a duty cycle $\beta_{FR} = \beta_{FL} = \beta_{HR} = \beta_{HL} = 0.55$, equal for the hind and forelimbs, and $t_i = [0.7; 0.2; 0.2; 0.7]$ (Figure 10). The contact forces are instead shown in Figure 11, and the friction coefficients in Figure 12. It can be observed how the normal forces F_{z_i} have a flat double-hump time history, typical of quadrupeds' locomotion [2,35]. All other significant parameters are shown in Table 1.

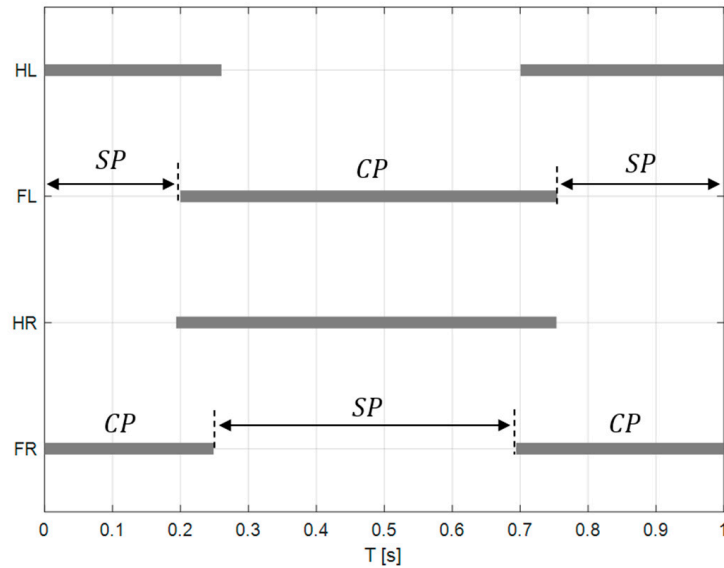


Figure 10. Gait sequence of the optimal walking trot solution: FL (front left), FR (front right), HL (hind left), HR (hind right), CP (contact phase), and SP (swing phase).

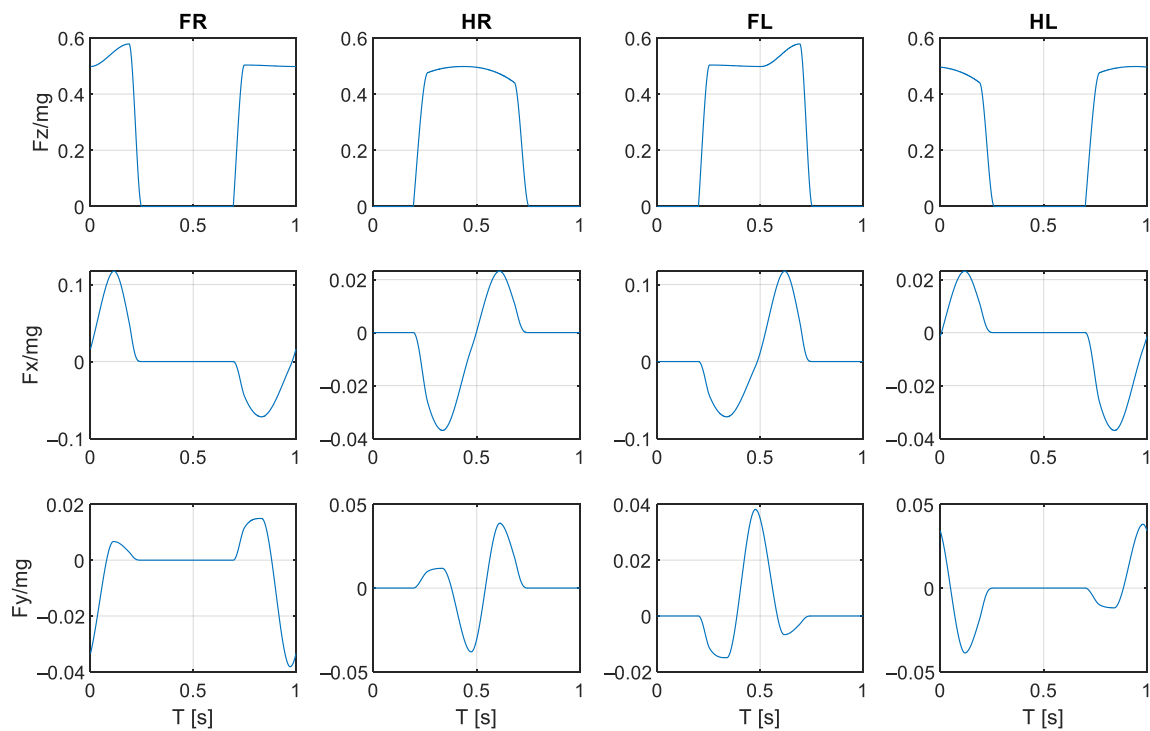


Figure 11. Contact forces normalized over the body weight.

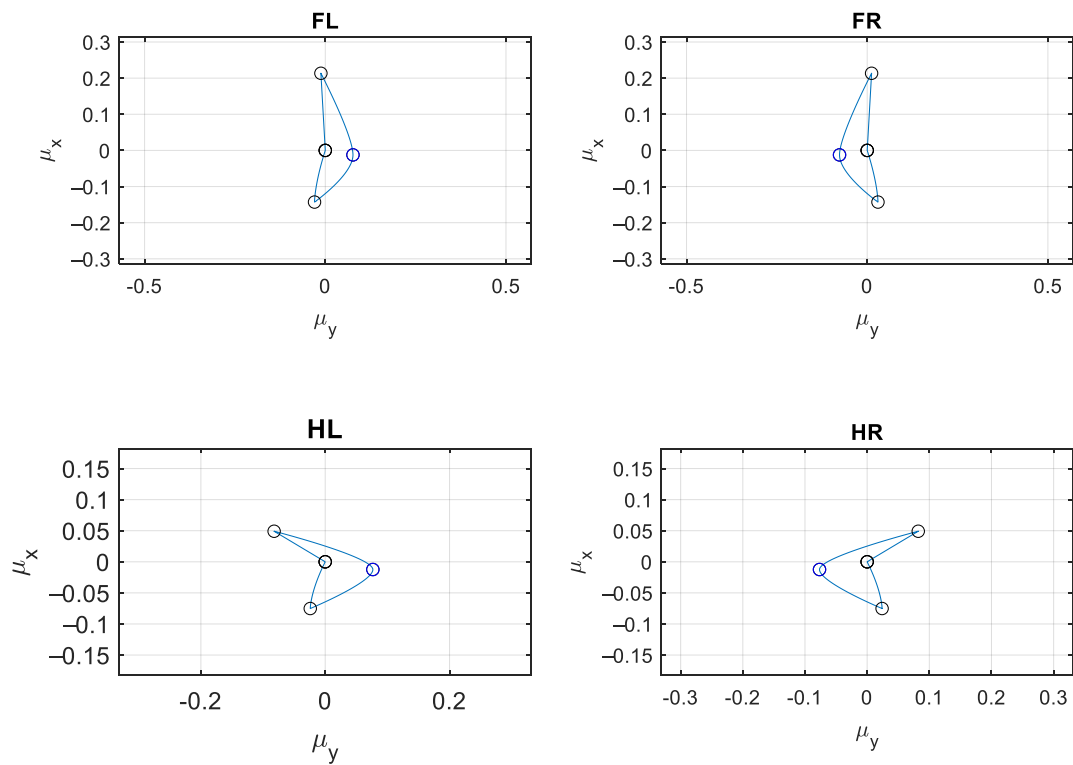


Figure 12. The trend of the coefficient of adhesion for each foot.

Table 1. Simulation setting parameters and results.

Parameter	Value	Unit
m	520	kg
m_p	26	kg
I_x	103	kg m ²
I_y	26.2	kg m ²
I_z	103	kg m ²
L	1.44	m
h	1	m
T	1	s
V	1.35	m/s
$\Delta x_{FR,FL_{max}} ; \Delta x_{FR,FL_{min}}$	1.08; 0.27	m
$\Delta x_{HR,HL_{max}} ; \Delta x_{HR,HL_{min}}$	-0.36; -1.17	m
$s_{FR} = s_{FL} = s_{HR} = s_{HL}$	0.81	m
x_0	0.36	m
y_0	0.0027	m
z_0	1	m
$\beta_{FR} = \beta_{FL} = \beta_{HR} = \beta_{HL}$	0.55	
$t_{FR} = t_{HL}$	0.7	s
$t_{FL} = t_{HR}$	0.2	s

In Figure 13 we can see the trajectory performed by the foot FR during one complete cycle.

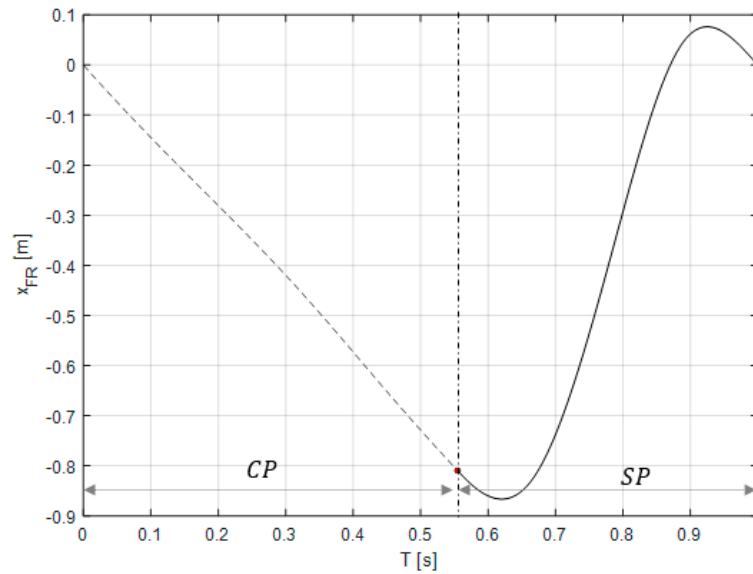


Figure 13. FR foot trajectory during contact and swing phase starting from t_{FR} .

To better assess the variability of the results, a statistical analysis on 10 runs of the optimization algorithm was performed. In all cases, the best gait found was the walking-trot and the ratio between the value of the objective function and its average differs by a maximum of 2.5%, as observed in Figure 14.

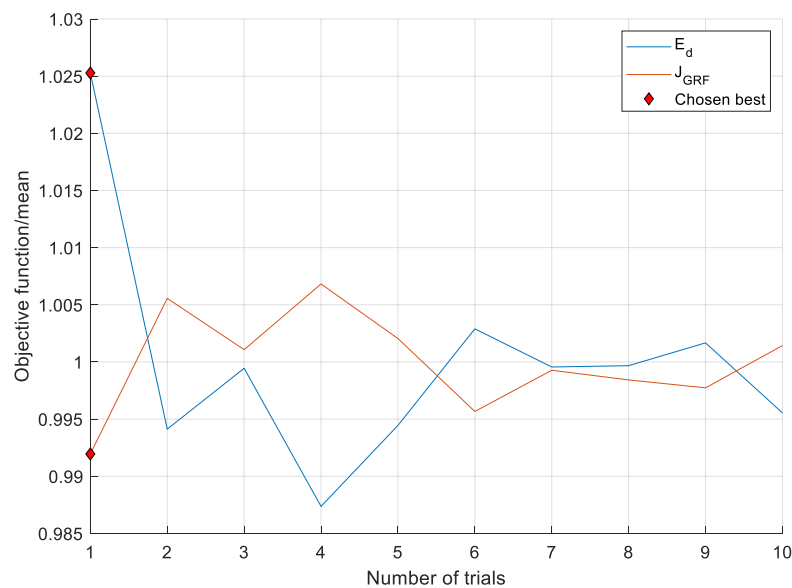


Figure 14. Comparison of fitness functions over the mean value between 10 trials.

Eventually, a comparison between the cumulative mechanical energy of the experimental and numerical optimization data is shown in Figure 15. For the experimental campaign [34], a group of horses with a weight ranging between 417 and 673 kg, was used. For each animal, ten sequences were considered within the speed range from 0.7 to 1.9 m/s. Five markers, positioned along the horses’ backbones, identify the vertical and longitudinal motion of their center of mass (CoM_{rigid}). The considered mechanical energy is defined by the expression (a special case of expression (29)):

$$E_{CoM_{rigid}} = \int_0^T |F_z \dot{z}| + |F_x \dot{x}| + mg|\dot{z}| dt \tag{33}$$

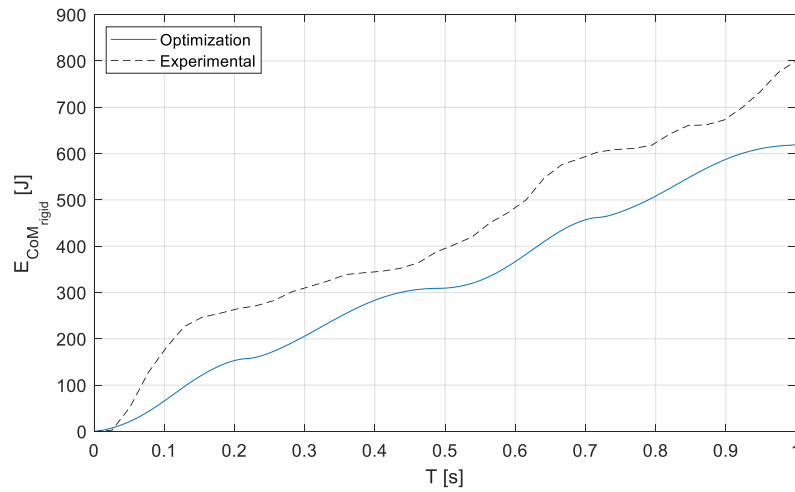


Figure 15. Mechanical energy comparison between experimental data and the optimal solution.

It is clear how the resulting energies are comparable.

4.2. Gaits Analysis for Different Speed and Cycle Duration T

The optimization solutions are tested for different speeds and cycle period T .

Figure 16 depicts the trend of the walking gait representing E_d , following Equation (30), as dependent on the cycle duration, for different speeds between 0.7 and 2 m/s. This map permits finding natural associations between convenient gait period and body velocity, to obtain gaits with a reasonably limited energy cost and smooth forces.

We notice that for $T < 0.5$ s the total energy is very large, because the swing phase has a very limited duration, needing very high energy to relocate the foot at its initial position. On the other hand, at high values for T , again the energy cost increases. Therefore, the map suggests that for any desired speed, there is an intermediate region for the gait period that allows a low energy consumption. Minimum energy expenditures are identified at $T = 1.25$ s for speed 1.35 m/s, at $T = 1$ s for speed 2 m/s, and $T = 1.66$ s for speed 0.7 m/s (blue square, green triangle, and red diamond, respectively).

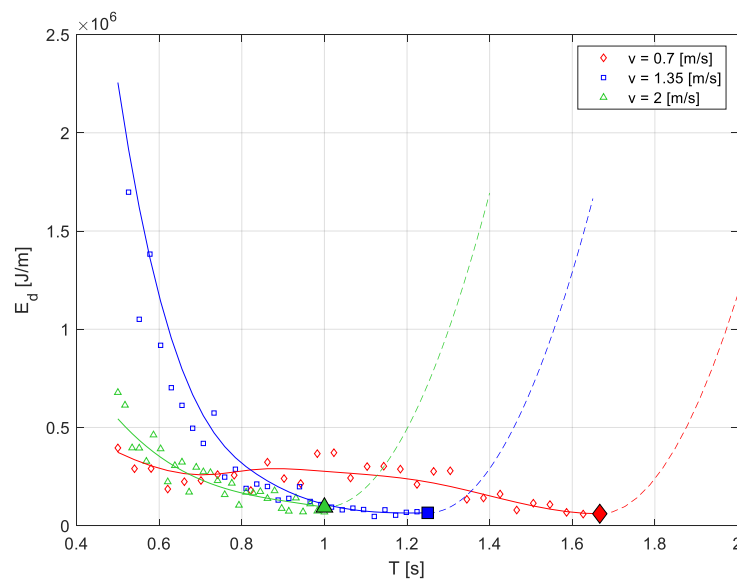


Figure 16. Walk gait energy E_d for different speeds and time cycles T .

In Figure 17, the trend of the trot gait is depicted. We notice the same behavior of low energy cost for the walking gait in the middle region, with an optimal association between periods and speed: $T = 1.25$ s for 1.35 m/s, $T = 1$ s for 2 m/s, and $T = 1.66$ s for 0.7 m/s.

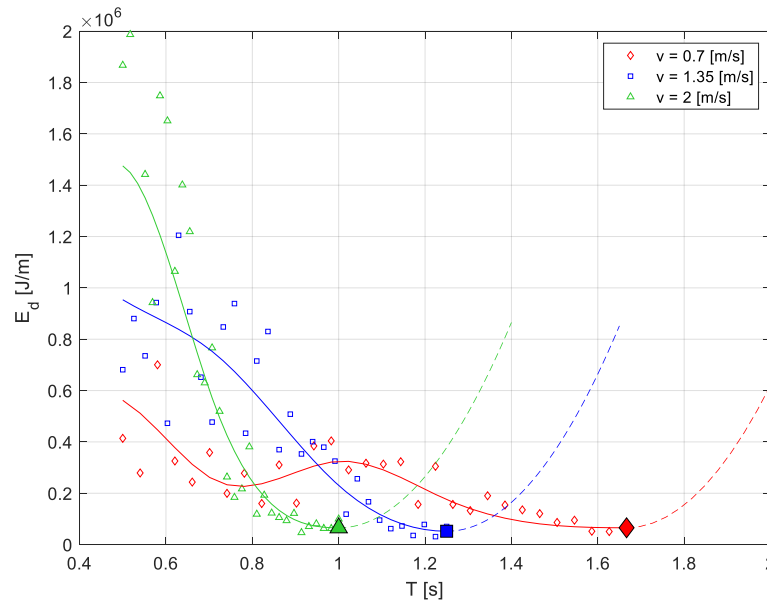


Figure 17. Trot gait energy E_d for different speeds and time cycles T .

Then, taking the minimum points for each gait and comparing them with the energy cost and jerk performances (Figure 18), we see how the transition between walking and trotting takes place at a speed between 0.7 m/s and 1.35 m/s, by using a Pareto criterion. In fact, for the lowest speed, 0.7 m/s, the walk is optimal, in a Pareto sense, since energy cost is lower, and jerk substantially similar. Increasing the speed at 1.35 m/s, a trot performs much better, since both energy and jerk indexes are lower with respect to the walking gait. For higher speeds, the trend of the two curves shows the trot gait is better than walking.

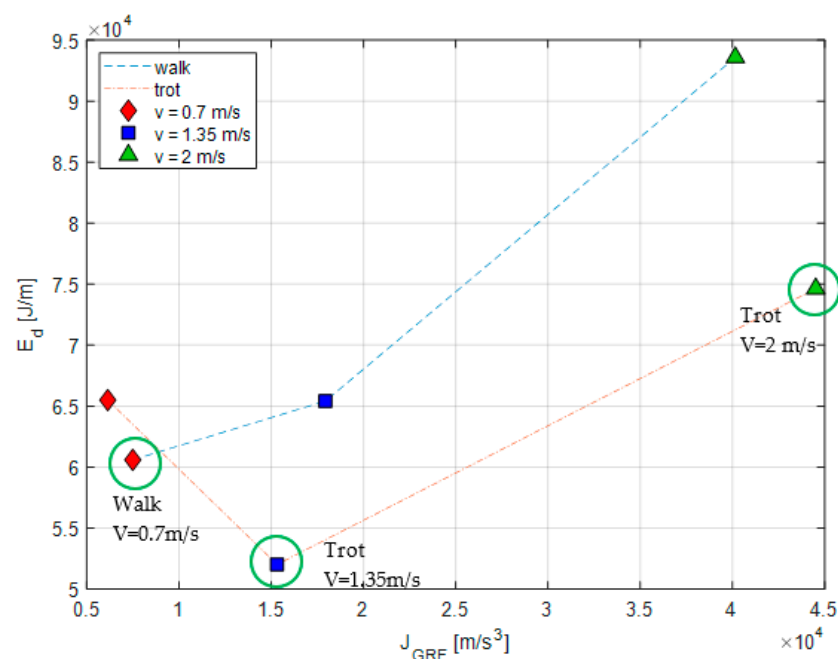


Figure 18. Gait transition from walk to trot based on Pareto’s frontier analysis.

5. Discussion

Based on the previous models and results, we can conjecture the optimal gait observed in nature can be derived as an evolutionary effect that combines minimum energy requirements and minimum jerk contact forces, to obtain a gait that is energy-saving and with a moderated mechanical impact on the legs articulations. This point of view has importance also for a quadrupedal robot design that would be aimed at imitating or even enhancing nature's results.

Nevertheless, the previous analysis introduces several approximations with related inaccuracies in the representation of quadrupedal mechanics.

As a first remark, dissipation effects are not taken into considerations. Credible dissipation models need indeed a fine-tuning and require specific and non-trivial experimental tests. This approximation introduces larger errors when increasing the leg's speed since the non-modeled effects of dissipation increase with some power of the velocity. Furthermore, one of the advantages of the previous analysis is the absence of a detailed leg model, that is on the other hand a limitation in the accuracy of the model. Additionally, the absence of a head in the model and its coordinated motion with legs is another approximation when analyzing the quadruped gaits.

Finally, the presence of flexible and deformable elements in the animal mechanical structure is not considered in the model, and these elements absorb elastic energy that plays a role in the global energy balance.

Actuators and their related power are not explicitly included in the animal mechanical model. Besides their obvious importance in the energy balance in the robot design, they guarantee the optimal gait is suitably tracked by the leg motion, with no obvious implications for their performances in terms of supplied maximum force and power, weights, and volumes.

Finally, the contact model is an approximate empirical model, and it will be necessary to check its reliability on the experimental ground.

Future work challenges will be related to overcoming these limitations. More specifically related to quadruped robot design implications, the kinematics and dynamics of leg implementation will be further optimized to be able to pursue the trajectories determined by the optimal gait generator. Non-linear optimal control algorithms recently developed by the authors [36,37] will be used to track kinematic references and forces exchanged on the ground. Such algorithms can be combined with reference trajectory generators [38,39] but can also incorporate the dynamics model and the power actuators by variational feedback control methods [40,41]. Therefore, it is possible to verify and confirm the validity of the results and then extend the work to the optimization of speed changes, changes of gaits, changes of direction, and optimal handling in the presence of obstacles and irregularities of the terrain [42,43].

The present analysis lays the groundwork for the design of new highly efficient quadrupedal robots.

6. Conclusions

This paper presents an investigation related to the optimal gaits for a quadrupedal robot. The interest of this analysis clearly relies on the use of such legged robots in many engineering areas, where the replacement of wheels by legs is highly desirable in an environmental scenario that has an uneven ground with obstacles and in the absence of specific infrastructure that permits a wheeled robot to operate comfortably.

The analysis presents several elements of originality. The optimal gait problem is formulated independently of any specific architecture for the leg mechanisms. The focus is the leg-ground reaction forces that control the quadruped's body motion. A detailed analysis of the contact introduces constitutive relationships for the reaction forces that permit their use in the formulation of the dynamic equation of the body. With the help of the periodicity conditions, that characterize the state variables of the robot involved in its gait and using them an initial guess based on a linearization of the equation of motion,

a GA optimization algorithm produces the optimal gaits of the quadruped. A multi-objective function introduces two basic principles of optimization. The first relies on the minimization of the maximum actuators' power and energy consumption. The second relies on the minimization of the contact jerks; that implies a requirement for preventing overload and stressful conditions for the robot mechanisms and its kinematic joints. Their combination, subjected to the Pareto frontier analysis, suggests optimal gaits.

The method is applied to a quadruped the size and mass of which are those of a horse, and the optimal gaits obtained by this optimization method are compared with results found in the technical literature for a real animal. The comparison shows that the different gaits, such as walk and trot, and the convenient transition from the first to the second, depends on the desired speed of the quadruped. The need for a transition comes out as a requirement of energy and jerk optimization; when the speed overcomes a given threshold (located between 0.7 m/s and 1.35 m/s) it is clearly convenient to change the gait. One may speculate this result could explain the origin of the quadruped gaits, as driven by nature, under a very long evolutionary process.

Author Contributions: The optimal gaits of a quadruped robot are part of the Ph.D. Thesis of M.L., under the guidance of G.P. (tutor). The methodology and conceptualization are by G.P. and M.L.; software, and validation, are by M.L. and G.P.; initial suggestions and some conceptualizations about optimal gait problem are by A.C., supervisor of the thesis project, who edited the writing of the manuscript and by N.P.B., former professor at Sapienza, now at University Roma 3. All authors have read and agreed to the published version of the manuscript.

Funding: This research received no external funding.

Institutional Review Board Statement: Not applicable.

Informed Consent Statement: Not applicable.

Conflicts of Interest: The authors declare no conflict of interest.

References

1. Srinivasan, M.; Ruina, A. Computer optimization of a minimal biped model discovers walking and running. *Nature* **2006**, *439*, 72–75. [[CrossRef](#)]
2. Dentinger, J.; Street, G. *Animal Locomotion*, 2nd ed.; Biewener, A.A., Patek, S.N., Eds.; Oxford University Press: Oxford, UK, 2018; p. 240. ISBN 978-019874316.
3. Alexander, R.M. Why Mammals Gallop1. *Am. Zool.* **1988**, *28*, 237–245. [[CrossRef](#)]
4. Al-dabbagh, A.H.A.; Ronsse, R. A review of terrain detection systems for applications in locomotion assistance. *Robot. Auton. Syst.* **2020**, *133*, 103628. [[CrossRef](#)]
5. Shen, T.; Afsar, M.R.; Haque, M.R.; McClain, E.; Meek, S.; Shen, X. A Human-assistive Robotic Platform with Quadrupedal Locomotion*. In Proceedings of the 2019 IEEE 16th International Conference on Rehabilitation Robotics (ICORR), Toronto, ON, Canada, 24–28 June 2019; pp. 305–310.
6. Hyun, D.J.; Park, H.; Ha, T.; Park, S.; Jung, K. Biomechanical design of an agile, electricity-powered lower-limb exoskeleton for weight-bearing assistance. *Robot. Auton. Syst.* **2017**, *95*, 181–195. [[CrossRef](#)]
7. Hu, L.; Zhou, C. EDA-Based optimization and learning methods for biped gait generation. *Lect. Notes Control Inf. Sci.* **2007**, *362*, 541–549.
8. Zhai, S.; Jin, B.; Cheng, Y. Mechanical design and gait optimization of hydraulic hexapod robot based on energy conservation. *Appl. Sci.* **2020**, *10*, 3884. [[CrossRef](#)]
9. Miandoab, S.N.; Kiani, F.; Uslu, E. Generation of Automatic Six-Legged Walking Behavior Using Genetic Algorithms. In Proceedings of the 2020 International Conference on INnovations in Intelligent SysTems and Applications (INISTA), Novi Sad, Serbia, 24–26 August 2020; pp. 1–5.
10. Kelasidi, E.; Jesmani, M.; Pettersen, K.Y.; Gravdahl, J.T. Locomotion efficiency optimization of biologically inspired snake robots. *Appl. Sci.* **2018**, *8*, 80. [[CrossRef](#)]
11. Zeng, X.; Zhang, S.; Zhang, H.; Li, X.; Zhou, H.; Fu, Y. Leg trajectory planning for quadruped robots with high-speed trot gait. *Appl. Sci.* **2019**, *9*, 1508. [[CrossRef](#)]
12. Masuri, A.; Medina, O.; Hacohen, S.; Shvalb, N. Gait and Trajectory Optimization by Self-Learning for Quadrupedal Robots with an Active Back Joint. *J. Robot.* **2020**, *2020*, 8051510. [[CrossRef](#)]
13. Meng, X.; Wang, S.; Cao, Z.; Zhang, L. A review of quadruped robots and environment perception. In Proceedings of the 2016 35th Chinese Control Conference (CCC), Chengdu, China, 27–29 July 2016; pp. 6350–6356.

14. Yang, K.; Rong, X.; Zhou, L.; Li, Y. Modeling and analysis on energy consumption of hydraulic quadruped robot for Optimal Trot motion control. *Appl. Sci.* **2019**, *9*, 1771. [[CrossRef](#)]
15. Kato, T.; Shiromi, K.; Nagata, M.; Nakashima, H.; Matsuo, K. Gait pattern acquisition for four-legged mobile robot by genetic algorithm. In Proceedings of the IECON 2015—41st Annual Conference of the IEEE Industrial Electronics Society, Yokohama, Japan, 9–12 November 2015; pp. 004854–004857.
16. Koco, E.; Glumac, S.; Kovacic, Z. Multiobjective optimization of a quadruped robot gait. In Proceedings of the 22nd Mediterranean Conference on Control and Automation, Palermo, Italy, 16–19 June 2014; pp. 1520–1526.
17. Luneckas, M.; Luneckas, T.; Udris, D.; Plonis, D.; Maskeliunas, R.; Damasevicius, R. Energy-efficient walking over irregular terrain: A case of hexapod robot. *Metrol. Meas. Syst.* **2019**, *26*, 645–660.
18. Luneckas, M.; Luneckas, T.; Udris, D.; Plonis, D.; Maskeliunas, R.; Damasevicius, R. A hybrid tactile sensor-based obstacle overcoming method for hexapod walking robots. *Intell. Serv. Robot.* **2020**. [[CrossRef](#)]
19. Focchi, M.; Del Prete, A.; Havoutis, I.; Featherstone, R.; Caldwell, D.; Semini, C. High-slope Terrain Locomotion for Torque-Controlled Quadruped Robots. *Auton. Robot.* **2016**, *41*, 259–272. [[CrossRef](#)]
20. Cai, C.; Jiang, H. Performance Comparisons of Evolutionary Algorithms for Walking Gait Optimization. In Proceedings of the 2013 International Conference on Information Science and Cloud Computing Companion, Guangzhou, China, 7–8 December 2013; pp. 129–134.
21. Srisuchinnawong, A.; Shao, D.; Ngamkajornwivat, P.; Teerakittikul, P.; Dai, Z.; Ji, A.; Manoonpong, P. Neural Control for Gait Generation and Adaptation of a Gecko Robot. In Proceedings of the 2019 19th International Conference on Advanced Robotics (ICAR), Belo Horizonte, Brazil, 2–6 December 2019; pp. 468–473.
22. Rubeo, S.; Szczecinski, N.; Quinn, R. A synthetic nervous system controls a simulated cockroach. *Appl. Sci.* **2017**, *8*, 6. [[CrossRef](#)]
23. Ma, W.-L.; Hamed, K.A.; Ames, A.D. First Steps Towards Full Model Based Motion Planning and Control of Quadrupeds: A Hybrid Zero Dynamics Approach. *arXiv* **2019**, arXiv:1909.08124.
24. Ren, D.; Shao, J.; Sun, G.; Shao, X. The complex dynamic locomotive control and experimental research of a quadruped-robot based on the robot trunk. *Appl. Sci.* **2019**, *9*, 3911. [[CrossRef](#)]
25. Griffin, T.; Main, R.; Farley, C. Biomechanics of quadrupedal walking: How do four-legged animals achieve inverted pendulum-like movements? *J. Exp. Biol.* **2004**, *207*, 3545–3558. [[CrossRef](#)]
26. Hobbs, S.J.; Levine, D.; Richards, J.; Clayton, H.; Tate, J.; Walker, R. Motion analysis and its use in equine practice and research. *Wien. Tierärztliche Mon.* **2010**, *97*, 55–64.
27. Yu, Z.; Zhou, Q.; Chen, X.; Li, Q.; Meng, L.; Zhang, W.; Huang, Q. Disturbance Rejection for Biped Walking Using Zero-Moment Point Variation Based on Body Acceleration. *IEEE Trans. Ind. Inf.* **2019**, *15*, 2265–2276. [[CrossRef](#)]
28. Baskoro, A.S.; Priyono, M.G. Design of humanoid robot stable walking using inverse kinematics and zero moment point. In Proceedings of the 2016 International electronics symposium (IES), Denpasar, Indonesia, 29–30 September 2016; pp. 335–339.
29. Gritli, H.; Belghith, S. Walking dynamics of the passive compass-gait model under OGY-based state-feedback control: Analysis of local bifurcations via the hybrid Poincaré map. *Chaos Solitons Fractals* **2017**, *98*, 72–87. [[CrossRef](#)]
30. Znegui, W.; Gritli, H.; Belghith, S. Stabilization of the passive walking dynamics of the compass-gait biped robot by developing the analytical expression of the controlled Poincaré map. *Nonlinear Dyn.* **2020**, *101*, 1061–1091. [[CrossRef](#)]
31. Roan, P.R.; Burmeister, A.; Rahimi, A.; Holz, K.; Hooper, D. Real-world validation of three tipover algorithms for mobile robots. In Proceedings of the 2010 IEEE International Conference on Robotics and Automation, Anchorage, AK, USA, 3–7 May 2010; pp. 4431–4436.
32. Konak, A.; Coit, D.W.; Smith, A.E. Multi-objective optimization using genetic algorithms: A tutorial. *Reliab. Eng. Syst. Saf.* **2006**, *91*, 992–1007. [[CrossRef](#)]
33. Tamaki, H.; Kita, H.; Kobayashi, S. Multi-objective optimization by genetic algorithms: A review. In Proceedings of the IEEE International Conference on Evolutionary Computation, Nagoya, Japan, 20–22 May 1996; pp. 517–522.
34. Nauwelaerts, S.; Kaiser, L.; Malinowski, R.; Clayton, H.M. Effects of trunk deformation on trunk center of mass mechanical energy estimates in the moving horse, *Equus caballus*. *J. Biomech.* **2009**, *42*, 308–311. [[CrossRef](#)] [[PubMed](#)]
35. Basu, C.; Wilson, A.M.; Hutchinson, J.R. The locomotor kinematics and ground reaction forces of walking giraffes. *J. Exp. Biol.* **2019**, *222*, 308–311. [[CrossRef](#)] [[PubMed](#)]
36. Pepe, G.; Antonelli, D.; Nesi, L.; Carcaterra, A. Flop: Feedback local optimality control of the inverse pendulum oscillations. In Proceedings of the ISMA 2018—International Conference on Noise and Vibration Engineering and USD 2018—International Conference on Uncertainty in Structural Dynamics, Leuven, Belgium, 17–19 September 2018; pp. 93–106.
37. Pepe, G.; Mezzani, F.; Carcaterra, A.; Cedola, L.; Rispoli, F. Variational control approach to energy extraction from a fluid flow. *Energies* **2020**, *13*, 4913. [[CrossRef](#)]
38. Antonelli, D.; Nesi, L.; Pepe, G.; Carcaterra, A. A novel approach in Optimal trajectory identification for Autonomous driving in racetrack. In Proceedings of the 2019 18th European Control Conference (ECC), Naples, Italy, 25–28 June 2019; pp. 3267–3272.
39. Antonelli, D.; Nesi, L.; Pepe, G.; Carcaterra, A. A novel control strategy for autonomous cars. In Proceedings of the 2019 American Control Conference (ACC), Philadelphia, PA, USA, 10–12 July 2019; pp. 711–716.
40. Antonelli, D.; Nesi, L.; Pepe, G.; Carcaterra, A. IMechatronic control of the car response based on VFC. In Proceedings of the ISMA 2018—International Conference on Noise and Vibration Engineering and USD 2018—International Conference on Uncertainty in Structural Dynamics, Leuven, Belgium, 17–19 September 2018; pp. 79–92.

41. Pepe, G.; Roveri, N.; Carcaterra, A. Experimenting Sensors Network for Innovative Optimal Control of Car Suspensions. *Sensors* **2019**, *19*, 3062. [[CrossRef](#)]
42. Pepe, G.; Laurenza, M.; Antonelli, D.; Carcaterra, A. A new optimal control of obstacle avoidance for safer autonomous driving. In Proceedings of the 2019 AEIT International Conference of Electrical and Electronic Technologies for Automotive (AEIT AUTOMOTIVE), Torino, Italy, 2–4 July 2019; pp. 1–6.
43. Laurenza, M.; Pepe, G.; Antonelli, D.; Carcaterra, A. Car collision avoidance with velocity obstacle approach: Evaluation of the reliability and performance of the collision avoidance maneuver. In Proceedings of the 5th International Forum on Research and Technologies for Society and Industry: Innovation to Shape the Future, RTSI 2019—Proceedings, Florence, Italy, 9–12 September 2019; pp. 465–470.